sciendo

DOI 10.2478/ama-2023-0060

acta mechanica et automatica, vol.17 no.4 (2023)

INFLUENCE OF THE MANIPULATOR CONFIGURATION ON VIBRATION EFFECTS

Paulina PIETRUŚ*, Piotr GIERLAK*

*Rzeszów University of Technology, Faculty of Mechanical Engineering and Aeronautics,
Department of Applied Mechanics and Robotics,
al. Powstańców Warszawy 12, 35-959 Rzeszów, Poland

p.pietrus@prz.edu.pl, pgierlak@prz.edu.pl

received 28 December 2022, revised 15 May 2023, accepted 24 May 2023

Abstract: Vibration analysis of industrial robots is one of the key issues in the context of robotisation of machining processes. Low-frequency vibrations result from flexibility in manipulator joints. Within the scope of the article, a model of a two-link robot manipulator was built. Dynamic equations of motion were formulated to study the influence of the robot arm configuration on vibration effects. Based on numerical simulations, the frequency spectrum of vibrations of the robot's links was determined, and tests were carried out in a number of configurations, obtaining a map of resonant frequencies depending on the configuration of the manipulator. Experimental studies were then carried out, which confirmed the conclusions from the simulation studies. The results obtained confirm that the positioning of the manipulator's links has a significant effect on vibration effects. Tests conducted using a vision system with a motion amplification application made it easier to interpret the results. The formulated mathematical model of the manipulator generates results that coincide with the results of experimental studies.

Key words: industrial manipulator, manipulator model, robot vibration

1. INTRODUCTION

Nowadays, industrial robots are increasingly used in many sectors of industry, such as machining, assembly and welding processes. For machining operations, industrial robots provide an economical and flexible alternative to standard CNC machine tools [1]. Machining operations performed by CNC machine tools provide greater accuracy and process stability. However, their maintenance costs are higher, and their movement capabilities are lower than those of robots. Therefore, CNC machines are often replaced by industrial robots [2]. The studies in Ref [2, 3] present general technical limitations of robots that occur during robotic machining processes, that is, accuracy, flexibility and possibility of excitation of robot resonant frequencies. The stability of operation during robotic machining is related to the stiffness of the robot and the vibrations that occur during machining. Therefore, research is being conducted to reduce the impact of negative effects occurring during robotic machining processes, among others vibrations. The most common applications of robots in machining processes include grinding, deburring and milling in soft materials [4, 5]. Proper planning of these processes requires the knowledge of the dynamic properties of the robot, so as not to excite, for example, its resonant vibrations. Identification of a mathematical model of the robot's mechanical structure is possible in the following experiments: modal analysis, measurement of the stiffness of the robot's structural elements and measurement of the stiffness in the manipulator's workspace [1]. Based on a review of existing solutions, examples of the application of the modal analysis of ABB and KUKA robots were found. In the studies in Ref [1, 6, 7, 8], modal analysis of KUKA manipulators was carried out to determine the frequencies of resonant vibrations. Impulse excitation generated using an impact hammer was used to excite the vibration, and the frequency response function was determined. The presented studies showed the dependence of the effect of the position of the robot arm on the excited natural frequencies. The studies in Ref [2, 8] presented an experimental modal analysis for an ABB manipulator. The study in Ref [9] extends the frequency determination problem to include an uncertainty analysis of the determination of resonance zones. The study in Ref [10] allows the determination of modal parameters of robots under static conditions. The study in Ref [8] presents a position-dependent control methodology to actively damp end effector vibration during robotic machining processes. The study in Ref [11] presents a hybrid vibration control of an industrial composite robotic manipulator based on a reduced order model. In the study in Ref [12], a method using machine intelligence was used to control the open-loop vibration of manipulators.

There are three main approaches to modelling the dynamics of industrial robots: modelling the robot as a system of rigid bodies with no flexibility and no joint backlash [13, 14], modelling with flexibility and backlash in joints [15, 16, 17, 18] and modelling with link flexibility [19, 20, 21]. The study in Ref [22] presents a modified method of modelling flexible robotic manipulators for use in dynamic analysis.

Models of manipulators, taking into account the flexibility of the joints [23], created for control purposes include a model of the drives, and then an underactuated system is obtained. The study of such a model is complex because, in addition to the movement of the arm, there are vibration phenomena and a complex problem of motion control. Modal models are also built based on the results of the experiments [24]. The aim of this study is to create the simplest possible analytical model of a robot that takes into account the vibration phenomena at selected positions of the robot

DOI 10.2478/ama-2023-0060

arm, without taking into account the influence of the arm movement on the vibration.

The article presents a model of a two-link robot manipulator, taking into account the flexibility of joints. The dynamic equations of motion of the manipulator were formulated using the Lagrangian approach. The purpose of the modelling was to determine the effect of the robot arm configuration on vibration effects. Due to the complexity of the equations of motion, properties were studied using numerical methods. The frequency spectrum of vibrations of the robot's links was determined. The study was carried out in many configurations, obtaining a map of resonant frequencies depending on the configuration of the robot. The results of theoretical analysis were confirmed by the results of a number of experimental tests. The main contribution of the research is the determination of the frequencies and modes of resonant vibrations using the experimental method and the formulation of a mathematical model of the dynamics of the robot arm, taking into account the flexibility of the joints.

The purpose of the modal analysis presented in this article is to determine the value of the resonant frequency and its dependence on the current position of the robot. The variability of the values of the resonant frequencies can lead to their activation in certain configurations, although the parameters of the processes to be carried out remain constant. The knowledge of the dynamic properties of the robot, which are of a vibrational nature, makes it possible to avoid resonances by correctly designing the robotic processes. This applies, for example, to robotic machining.

In the case of a typical industrial robot with six degrees of freedom, there will be no new phenomena, but there will be an accumulation of those that are present in a two-part robot. Hence, the model will be qualitatively the same. This article, however, draws attention to the occurring phenomena and presents the possibilities of their analysis. The simplification of modelling only two degrees of freedom of the robot makes it easier to present the results and understand the analysed phenomena.

2. MODEL OF MANIPULATOR

To analyse the influence of the manipulator configuration on vibration effects, a model of a two-link planar manipulator was adopted, the schematic diagram of which is shown in Fig. 1. It consists of two articulated links that have the ability to move in the xy plane. The model takes into account the flexibility in joints A and B, which is the cause of low-frequency vibration of the manipulator. Point C is the end point of the arm, while points S1 and S2 are the centres of mass of links 1 and 2, respectively.

Low-frequency vibrations of robots result from flexibility in the joints, that is, at points A and B. They involve the rotational oscillatory motion of the links relative to the joints. To account for them, it can be assumed that each configuration coordinate, that is, q_1 and q_2, can be expressed as the sum of two angular values:

$$\begin{cases} q_1 = \beta_1 + \alpha_1 \\ q_2 = \beta_2 + \alpha_2 \end{cases} \tag{1}$$

where β_1 and β_2 are the values describing the positions of the manipulator's links, relative to which the oscillations of these links occur, expressed by the variables α_1 and α_2. In the ideal case, when no oscillations occur, β_1 and β_2 are simply the same as the configuration coordinates q_1 and q_2. When the flexibility in the joints is taken into account, the angles α_1 and α_2 are fast-variable values related to the vibration effects of the robotic arm, while β_1 and β_2 are slow-variable values whose changes result from the realisation of the motion trajectory, or alternatively, they are constant values if the robotic arm is in a fixed position.

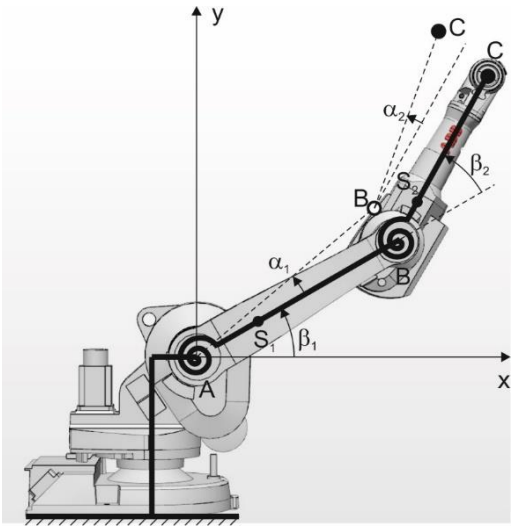

Fig. 1. A two-link planar manipulator with flexible joints

The equations of motion of the manipulator were formulated using the Lagrangian approach. For this purpose, the potential energy was determined first, followed by the kinetic energy of the manipulator.

The potential energy of the system is the sum of the potential energies of the masses in the earth's gravitational field and the potential energies of the elastic elements at the joints:

$$V = V_{k1} + V_{k2} + V_{g1} + V_{g2} \tag{2}$$

where V_{k1} and V_{k2} are the potential energies of the elastic joints of links 1 and 2, and V_{g1} and V_{g2} are the potential energies of the masses of links 1 and 2 in the gravitational field. They are described by the following equations:

$$V_{k1} = \frac{1}{2} k_1 (\alpha_1 + \alpha_{1st})^2 \tag{3}$$

$$V_{k2} = \frac{1}{2} k_2 (\alpha_2 + \alpha_{2st})^2 \tag{4}$$

$$V_{g1} = m_1 g l_{c1} sin(\beta_1 + \alpha_1) \tag{5}$$

$$V_{g2} = m_2 g [l_1 sin(\beta_1 + \alpha_1) + l_{c2} sin(\beta_1 + \beta_2 + \alpha_1 + \alpha_2)] \tag{6}$$

in which k_1 and k_2 are the elastic coefficients of the joints 1 and 2 (at points A and B), respectively; α_{1st} and α_{2st} are the static deformations of the joints under the influence of moments from the gravity forces of the links, m_1 and m_2 are the masses of links 1 and 2, respectively; l_1 is the length of link 1; and l_{c1} and l_{c2} are the distances of the centres of mass of the links from the joints (distances AS1 and BS2). The trigonometric functions appearing in Eqs. (5) and (6) can be decomposed as follows:

$$sin(\beta_1 + \alpha_1) = sin\,\beta_1\, cos\,\alpha_1 + cos\,\beta_1\, sin\,\alpha_1 = sin\,\beta_1 + \alpha_1\, cos\,\beta_1 \tag{7}$$

$$sin(\beta_1 + \beta_2 + \alpha_1 + \alpha_2) = sin(\beta_1 + \beta_2)\, cos(\alpha_1 + \alpha_2) + cos(\beta_1 + \beta_2)\, sin(\alpha_1 + \alpha_2) = sin(\beta_1 + \beta_2) + (\alpha_1 + \alpha_2)\, cos(\beta_1 + \beta_2) \tag{8}$$

where the following approximations are considered in the second step of the transformation: $\sin\alpha_1 = \alpha_1$, $\cos\alpha_1 = 1$, $\sin(\alpha_1 + \alpha_2) = \alpha_1 + \alpha_2$, $\cos(\alpha_1 + \alpha_2) = 1$. These are due to the fact that the angular coordinates α_1 and α_2 describing the vibration have small values. The total potential energy, taking into account the linearisation performed, is given as follows:

$$V = \frac{1}{2}k_1(\alpha_1^2 + 2\alpha_1\alpha_{1st} + \alpha_{1st}^2) + \frac{1}{2}k_2(\alpha_2^2 + 2\alpha_2\alpha_{2st} + \alpha_{2st}^2) + m_1 g l_{c1}(\sin\beta_1 + \alpha_1\cos\beta_1) + m_2 g l_1(\sin\beta_1 + \alpha_1\cos\beta_1) + m_2 g l_{c2}\sin(\beta_1 + \beta_2) + m_2 g l_{c2}(\alpha_1 + \alpha_2)\cos(\beta_1 + \beta_2) \quad (9)$$

The static deformations of the joints were determined using the Dirichlet criterion. For this purpose, the derivatives of the potential energy (9) were determined after the coordinates α_1 and α_1, which are equal to zero at the static equilibrium position defined by the values $\alpha_1 = \alpha_2 = 0$, that is, they satisfy the following conditions:

$$\left.\frac{\partial V}{\partial\alpha_1}\right|_{\alpha_1=0,\alpha_2=0} = k_1(\alpha_1 + \alpha_{1st}) + (m_1 g l_{c1} + m_2 g l_1)\cos\beta_1 + m_2 g l_{c2}\cos(\beta_1 + \beta_2) = 0 \quad (10)$$

$$\left.\frac{\partial V}{\partial\alpha_2}\right|_{\alpha_1=0,\alpha_2=0} = k_2(\alpha_2 + \alpha_{2st}) + m_2 g l_{c2}\cos(\beta_1 + \beta_2) = 0 \quad (11)$$

From Eqs. (10) and (11), static deformations were calculated as follows:

$$\alpha_{1st} = -\frac{(m_1 g l_{c1} + m_2 g l_1)}{k_1}\cos\beta_1 - \frac{m_2 g l_{c2}}{k_1}\cos(\beta_1 + \beta_2) \quad (12)$$

$$\alpha_{2st} = -\frac{m_2 g l_{c2}}{k_2}\cos(\beta_1 + \beta_2) \quad (13)$$

Taking into account the static deformations (12) and (13) in Eq. (9), and omitting α_{1st}^2 and α_{2st}^2 as small values of higher order than α_{1st} and α_{2st}, the potential energy can be written in the following form:

$$V = \frac{1}{2}k_1\alpha_1^2 + \frac{1}{2}k_2\alpha_2^2 + m_1 g l_{c1}\sin\beta_1 + m_2 g l_1\sin\beta_1 + m_2 g l_{c2}\sin(\beta_1 + \beta_2) \quad (14)$$

The kinetic energy of the system is the sum of the kinetic energies of all links:

$$E = E_1 + E_2 \quad (15)$$

where the kinetic energy of link 1 is the energy of the solid in rotation relative to point A:

$$E_1 = \frac{1}{2}I_A^{(1)}\dot{q}_1^2 \quad (16)$$

and the kinetic energy of link 2 is the energy of plane motion understood as the sum of the progressive motion of the link's centre of mass (point S2) and rotational motion relative to the link's centre of mass:

$$E_2 = \frac{1}{2}m_2 v_{S2}^2 + \frac{1}{2}I_{S2}^{(2)}(\dot{q}_1 + \dot{q}_2)^2 \quad (17)$$

Thus, the kinetic energy is as follows:

$$E = \frac{1}{2}I_A^{(1)}\dot{q}_1^2 + \frac{1}{2}m_2 v_{S2}^2 + \frac{1}{2}I_{S2}^{(2)}(\dot{q}_1 + \dot{q}_2)^2 \quad (18)$$

where $I_A^{(1)}$ is the mass moment of inertia of link 1 defined relative to point A and $I_{S2}^{(2)}$ is the mass moment of inertia of link 2 defined relative to the centre of mass of link 2.

A quasi-static case was further considered, in which the motions of the links described by the variables α_1 and α_2 were considered relative to the position of the links described by the coordinates β_1 and β_2. The coordinates β_1 and β_2 are treated as constants because their changes during movement are many times slower than those of α_1 and α_2. Therefore, based on these assumptions and Eq. (1), the angular velocities of the links are expressed as follows:

$$\begin{cases}\dot{q}_1 = \dot{\beta}_1 + \dot{\alpha}_1 = \dot{\alpha}_1 \\ q_2 = \dot{\beta}_2 + \dot{\alpha}_2 = \dot{\alpha}_2\end{cases} \quad (19)$$

where it is assumed that $\beta_1$and β_2 are constants. This assumption leads to the analysis of the vibration of the manipulator at the positions defined by the angles β_1 and β_2.

The coordinates of the centre of mass of link 2 are defined by the following formula:

$$\begin{cases}x_{S2} = l_1\cos(q_1) + l_{c2}\cos(q_1 + q_2) \\ y_{S2} = l_1\sin(q_1) + l_{c2}\sin(q_1 + q_2)\end{cases} \quad (20)$$

which, after taking into account Eq. (1), is written in the following form:

$$\begin{cases}x_{S2} = l_1\cos(\beta_1 + \alpha_1) + l_{c2}\cos(\beta_1 + \beta_2 + \alpha_1 + \alpha_2) \\ y_{S2} = l_1\sin(\beta_1 + \alpha_1) + l_{c2}\sin(\beta_1 + \beta_2 + \alpha_1 + \alpha_2)\end{cases} \quad (21)$$

After differentiating these equations with respect to time, the components of the velocity of the centre of mass of link 2 can be obtained:

$$\begin{cases}\dot{x}_{S2} = -l_1\dot{\alpha}_1\sin(\beta_1 + \alpha_1) - l_{c2}(\dot{\alpha}_1 + \dot{\alpha}_2)\sin(\beta_1 + \beta_2 + \alpha_1 + \alpha_2) \\ \dot{y}_{S2} = l_1\dot{\alpha}_1\cos(\beta_1 + \alpha_1) + l_{c2}(\dot{\alpha}_1 + \dot{\alpha}_2)\cos(\beta_1 + \beta_2 + \alpha_1 + \alpha_2)\end{cases} \quad (22)$$

while the square of the velocity value of point S2 is as follows:

$$v_{S2}^2 = \dot{x}_{S2}^2 + \dot{y}_{S2}^2 = l_1^2\dot{\alpha}_1^2 + l_{c2}^2(\dot{\alpha}_1 + \dot{\alpha}_2)^2 + 2l_1 l_{c2}\dot{\alpha}_1(\dot{\alpha}_1 + \dot{\alpha}_2)\cos(\beta_2 + \alpha_2) \quad (23)$$

Taking into account the kinematic relations, the kinetic energy can be written in the following form:

$$E = \frac{1}{2}\left[I_A^{(1)} + I_{S2}^{(2)} + m_2 l_1^2 + m_2 l_{c2}^2 + m_2 l_1 l_{c2}\cos(\beta_2 + \alpha_2)\right]\dot{\alpha}_1^2 + \left[m_2 l_{c2}^2 + m_2 l_1 l_{c2}\cos(\beta_2 + \alpha_2) + I_{S2}^{(2)}\right]\dot{\alpha}_1\dot{\alpha}_2 + \frac{1}{2}\left(m_2 l_{c2}^2 + I_{S2}^{(2)}\right)\dot{\alpha}_2^2 \quad (24)$$

The Lagrange function is introduced as follows:

$$L = E - V = \frac{1}{2}\left[I_A^{(1)} + I_{S2}^{(2)} + m_2 l_1^2 + m_2 l_{c2}^2 + m_2 l_1 l_{c2}\cos(\beta_2 + \alpha_2)\right]\dot{\alpha}_1^2 + \frac{1}{2}\left(m_2 l_{c2}^2 + I_{S2}^{(2)}\right)\dot{\alpha}_2^2 + \left[I_{S2}^{(2)} + m_2 l_{c2}^2 + m_2 l_1 l_{c2}\cos(\beta_2 + \alpha_2)\right]\dot{\alpha}_1\dot{\alpha}_2 - \frac{1}{2}k_1\alpha_1^2 - \frac{1}{2}k_2\alpha_2^2 - m_1 g l_{c1}\sin\beta_1 - m_2 g l_1\sin\beta_1 - m_2 g l_{c2}\sin(\beta_1 + \beta_2) \quad (25)$$

and then the Lagrange equations are formulated:

$$\begin{cases}\frac{d}{dt}\left(\frac{\partial L}{\partial\dot{\alpha}_1}\right) - \frac{\partial L}{\partial\alpha_1} = 0 \\ \frac{d}{dt}\left(\frac{\partial L}{\partial\dot{\alpha}_2}\right) - \frac{\partial L}{\partial\alpha_2} = 0\end{cases} \quad (26)$$

which describe the free vibration of the robot arm. Their detailed form is as follows:

$$\left[I_A^{(1)} + I_{S2}^{(2)} + m_2 l_1^2 + m_2 l_{c2}^2 + 2m_2 l_1 l_{c2}\cos(\beta_2 + \alpha_2)\right]\ddot{\alpha}_1 + \left[I_{S2}^{(2)} + m_2 l_{c2}^2 + m_2 l_1 l_{c2}\cos(\beta_2 + \alpha_2)\right]\ddot{\alpha}_2 -$$

DOI 10.2478/ama-2023-0060

$$2m_2 l_1 l_{c2} \sin(\beta_2 + \alpha_2)\dot{\alpha}_2 \dot{\alpha}_1 - m_2 l_1 l_{c2} \sin(\beta_2 + \alpha_2)\dot{\alpha}_2^2 + k_1\alpha_1 = 0$$

$$\left(I_{S2}^{(2)} + m_2 l_{c2}^2\right)\ddot{\alpha}_2 + \left[I_{S2}^{(2)} + m_2 l_{c2}^2 + m_2 l_1 l_{c2} \cos(\beta_2 + \alpha_2)\right]\ddot{\alpha}_1 + m_2 l_1 l_{c2} \sin(\beta_2 + \alpha_2)\dot{\alpha}_1^2 + k_2\alpha_2 = 0 \quad (27)$$

By grouping the individual expressions into matrices, the equation of motion was obtained in the general form given by the following equation:

$$\boldsymbol{M}\ddot{\boldsymbol{\alpha}} + \boldsymbol{C}\dot{\boldsymbol{\alpha}} + \boldsymbol{K}\boldsymbol{\alpha} = \boldsymbol{0} \quad (28)$$

in which matrices have the following form:

$$\boldsymbol{\alpha} = \begin{bmatrix} \boldsymbol{\alpha_1} \\ \boldsymbol{\alpha_2} \end{bmatrix} \quad (29)$$

$$\boldsymbol{M} = \begin{bmatrix} a_1 + 2a_2 \cos(\beta_2 + \alpha_2) & a_3 + a_2 \cos(\beta_2 + \alpha_2) \\ a_3 + a_2 \cos(\beta_2 + \alpha_2) & a_3 \end{bmatrix} \quad (30)$$

$$\boldsymbol{C} = \begin{bmatrix} -a_2 \sin(\beta_2 + \alpha_2)\dot{\alpha}_2 & -a_2 \sin(\beta_2 + \alpha_2)(\dot{\alpha}_1 + \dot{\alpha}_2) \\ a_2 \sin(\beta_2 + \alpha_2)\dot{\alpha}_1 & 0 \end{bmatrix} \quad (31)$$

$$\boldsymbol{K} = \begin{bmatrix} k_1 & 0 \\ 0 & k_2 \end{bmatrix} \quad (32)$$

while parameters a_i result from the following grouping of coefficients:

$$\begin{cases} a_1 = I_A^{(1)} + I_{S2}^{(2)} + m_2 l_1^2 + m_2 l_{c2}^2 \\ a_2 = m_2 l_1 l_{c2} \\ a_3 = I_{S2}^{(2)} + m_2 l_{c2}^2 \end{cases} \quad (33)$$

The trigonometric functions occurring in the model can be decomposed as follows:

$$\cos(\beta_2 + \alpha_2) = \cos\beta_2 \cos\alpha_2 - \sin\beta_2 \sin\alpha_2 \quad (34)$$

$$\sin(\beta_2 + \alpha_2) = \sin\beta_2 \cos\alpha_2 + \cos\beta_2 \sin\alpha_2 \quad (35)$$

For the purpose of research involving vibration analysis in selected robot configurations defined by angular coordinates β_1 and β_2, it can be assumed that the values of $\sin\beta_2$ and $\cos\beta_2$ are constant in each analysed configuration. Thus, the designations $b_1 = \sin\beta_2$, $b_2 = \cos\beta_2$ were introduced. From the fact that the angular coordinates α_1 and α_2 describing the oscillations are small angles, it follows that the following approximations can be used: $\sin\alpha_2 = \alpha_2$, $\cos\alpha_2 = 1$. Then the expressions described by Eqs. (34) and (35) can be written in the linearised form:

$$\cos(\beta_2 + \alpha_2) = b_2 - b_1\alpha_2 \quad (36)$$

$$\sin(\beta_2 + \alpha_2) = b_1 + b_2\alpha_2 \quad (37)$$

Introducing these designations into the dynamic equations of motion, the M and C matrices are written as follows:

$$\boldsymbol{M} = \begin{bmatrix} a_1 + 2a_2 b_2 - 2a_2 b_1 \alpha_2 & a_3 + a_2 b_2 - a_2 b_1 \alpha_2 \\ a_3 + a_2 b_2 - a_2 b_1 \alpha_2 & a_3 \end{bmatrix} \quad (38)$$

$$\boldsymbol{C} = \begin{bmatrix} -(a_2 b_1 + a_2 b_2 \alpha_2)\dot{\alpha}_2 & -(a_2 b_1 + a_2 b_2 \alpha_2)(\dot{\alpha}_1 + \dot{\alpha}_2) \\ (a_2 b_1 + a_2 b_2 \alpha_2)\dot{\alpha}_1 & 0 \end{bmatrix} \quad (39)$$

An important fact is that the angular coordinate β_1 does not appear in the obtained equations of motion, from which it follows that the angular position of link 1 does not affect the vibrations of the robot arm. However, they depend on the angular coordinate β_2.

Since the authors had a second manipulator, identical to the one studied in this article, and used it for detailed analyses of its structure, the masses and mass moments of inertia were determined experimentally. The lengths of the links were obtained from geometric measurements. The joint stiffness coefficients k_1 and k_2 were determined experimentally. The manipulator arm was loaded with known, successively increasing loads (from the weights suspended at the end of the arm), and the displacements of each manipulator joint were measured using a Leica AT 960 Laser Tracker (Fig. 2). This was used to determine the characteristics of the moments as a function of the angular displacements of the links. The characteristics were approximated by linear functions, which allowed the assumption of constant values for the stiffness coefficients given in Tab. 1.

Fig. 2. Measurement of displacements of links under the loads

Tab. 1. Coefficient values used in robot model

Coefficient	Unit	Value
$I_A^{(1)}$	kgm^2	0.55
$I_{S2}^{(2)}$	kgm^2	0.0009
m_2	kg	50.58
l_1	m	0.63
l_{c2}	m	0.1
k_1	Nm/rad	555,000
k_2	Nm/rad	138.000
β_1	rad	2π/3

3. ANALYTICAL SOLUTION

To analytically determine the resonant frequencies of the robot, simplifications were introduced into the equations of motion (28) to obtain linear equations. Firstly, the terms of the equations containing the angular velocities $\dot{\alpha}_i$ were omitted to eliminate the quadratic forms of the velocities. This is equivalent to omitting the C matrix. Furthermore, the influence of the angles α_i on the matrix M was omitted, justified by the relatively small influence of the angles α_i on the phenomena related to the inertia of the links compared to the influence of these angles on the phenomena related to the elasticity expressed by the $K\alpha$ term. The equation of

motion was thus obtained in the following form:

$$\boldsymbol{M}_0\ddot{\boldsymbol{\alpha}} + \boldsymbol{K}\boldsymbol{\alpha} = \boldsymbol{0} \tag{40}$$

where $\boldsymbol{M}_0 = \boldsymbol{M}(\boldsymbol{\alpha} = \boldsymbol{0}, \boldsymbol{\beta})$ was adopted. The matrix $\boldsymbol{M}_0$ is constant in a given configuration defined by the coordinate vector $\boldsymbol{\beta}$. The solution to the equation of motion (40) has the following form:

$$\alpha_i = A_i cos(\omega t + \varphi) \tag{41}$$

Substituting this solution and its second derivative into the equation of motion (40) gives the following algebraic equation:

$$(-\omega_0^2\boldsymbol{M}_0 + \boldsymbol{K})\boldsymbol{A} = \boldsymbol{0} \tag{42}$$

where $\boldsymbol{A}$ is the displacement amplitude vector of the form $\boldsymbol{A} = [A_1 \quad \dots \quad A_n]^T$. Eq. (42) is satisfied if

$$det(-\omega_0^2\boldsymbol{M}_0 + \boldsymbol{K}) = 0 \tag{43}$$

This is the equation for the natural frequencies of the system, which, in the case of the considered manipulator, has the following form:

$$(a_1a_3 - a_3^2 - a_2^2\cos^2\beta_2)\omega_0^4 - (a_1k_2 + 2a_2k_2\cos\beta_2 + a_3k_1)\omega_0^2 + k_1k_2 = 0 \tag{44}$$

The positive solutions of Eq. (44) are follows:

$$\omega_{0\,\{1,2\}} = \sqrt{\frac{d_1}{2d_2} \mp \sqrt{\frac{d_1^2}{4d_2^2} - \frac{k_1k_2}{d_2}}} \tag{45}$$

where $d_1 = a_1k_2 + 2a_2k_2\cos\beta_2 + a_3k_1$ and $d_2 = a_1a_3 - a_3^2 - a_2^2\cos^2\beta_2$ were adopted. Taking into account the values of the parameters a_1, a_2 and a_3 and the elasticity coefficients k_1 and k_2 (Tab. 1), the values of the natural frequencies $f_1 = \omega_{0\,1}/(2\pi)$ and $f_2 = \omega_{0\,2}/(2\pi)$ have been calculated as a function of the configuration determined by the β_2 coordinate for $\beta_2 \in \langle -2{,}269 \div 2{,}619 \rangle$ rad. The results of the calculations are shown in Fig. 3.

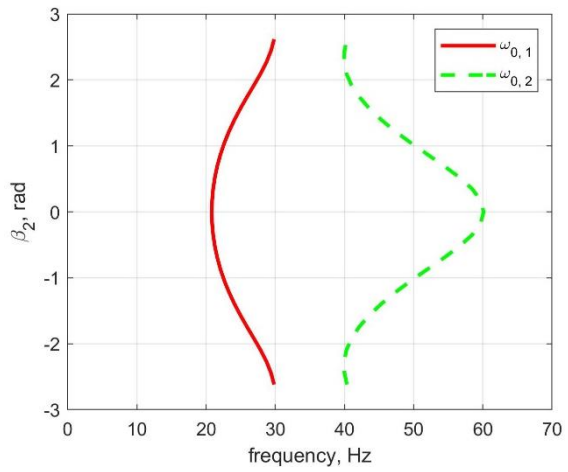

Fig. 3. Robot natural frequencies as a function of the β_2 angle, obtained from the analytical solution

Fig. 3 shows that the natural frequencies of the robot arm depend significantly on its positioning. As the absolute value of the angle β_2 increases, the value of the first natural frequency increases, while the value of the second natural frequency decreases. Changes in the frequencies of the natural vibrations in different positions of the robot result from changes in the inertia of the system since the M and C matrices depend on the position of link 2 with respect to link 1. The stiffness matrix, on the other hand, is constant regardless of the configuration. The first frequency increases and the second frequency decreases as the absolute value of the angle β_2 increases because the term $\frac{d_1^2}{4d_2^2} - \frac{k_1k_2}{d_2}$ in Eq. (45) decreases as the angle β_2 increases.

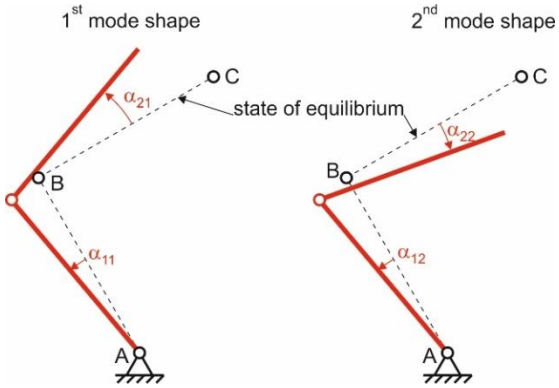

Fig. 4. Vibration mode shapes

The mode shapes of the robot arm vibrations are shown in Fig. 4. The first mode of vibration consists of the links rotating in the same direction, whereas the second mode consists of the links rotating in opposite directions.

4. NUMERICAL ANALYSIS

Due to the complexity of the equations of motion, it is not possible to obtain analytical forms of solutions without simplification. Therefore, the study of properties of Equ. (28) was carried out using numerical methods. Eq. (28) was transformed to the following form:

$$\ddot{\boldsymbol{\alpha}} = -\boldsymbol{M}^{-1}[\boldsymbol{C}\dot{\boldsymbol{\alpha}} + \boldsymbol{K}\boldsymbol{\alpha}] \tag{46}$$

Eq. (46) was solved numerically, assuming non-zero initial conditions causing vibrations with resonant frequencies. Then, the frequency spectrum of the vibrations of the robot's links, that is, the solutions of Eq. (46), was determined. Tests were carried out in many configurations obtaining a map of resonant frequencies depending on the robot's configuration. In the simulation studies (Tab. 1), the data corresponding to a section of the ABB IRB 1600 robot arm were adopted. The first link in the model corresponds to the second link of the IRB 1600 robot arm, and the second link in the model corresponds to the third link of the IRB 1600 robot.

Fig. 5 shows resonant frequency maps showing the vibration spectra of the robot's links as a function of the arm configuration defined by the angular coordinate β_2. This coordinate describes the angular position of link 2 relative to link 1. The characteristics show two resonant frequencies as the model takes into account the two degrees of freedom of the manipulator associated with vibration movements. The characteristics further show that the resonant frequencies of the robotic arm's vibration significantly depend on its positioning. As the absolute value of the angle β_2 increases, the value of the first resonant frequency increases, while the value of the second resonant frequency decreases, and significantly so.

DOI 10.2478/ama-2023-0060

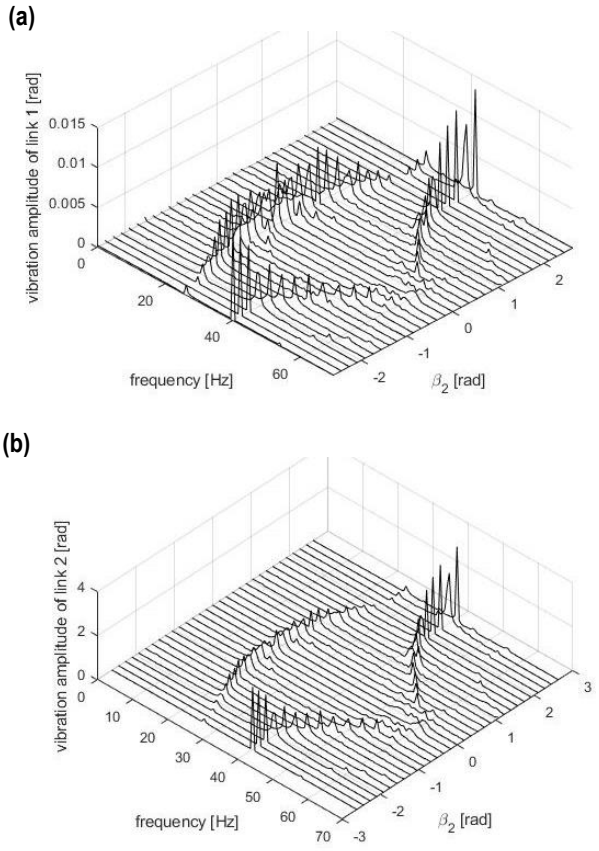

Fig. 5. Resonant frequency maps of the manipulator depending on the configuration: (a) vibration spectrum of link 1, (b) vibration spectrum of link 2

4. EXPERIMENTAL STUDIES

An ABB IRB 1600 robot (Fig. 6) was used in the experimental studies to verify the analytical modelling and simulation results. A PCB 086C03 soft-tipped impact hammer was used to excite the vibrations since the subject of the analysis was low-frequency vibrations of the manipulator related to flexibility in the joints. The point of application of the forcing was the robot's flange. The Iris M system, which includes a high-resolution camera and a computer with RDI Motion Amplification software, was used to record and analyse the robot's vibrations. The functionality of the system allows image acquisition and further processing, including amplification of the recorded motion and vibration analysis of selected regions (points) in the time and frequency domains.

The motion amplification function allows observation of displacements with amplitudes of several micrometres at multiple magnifications. On the other hand, vibration analysis of selected regions marked on the recorded image allows determining the motion parameters (displacement, velocity) at a given point and performing Fourier transformation of the motion parameters. In addition, the available filters allow separating each vibration frequency present and filtering the image in such a way as to observe each form of vibration of the robot separately. This functionality is particularly useful in the context of robot vibration analysis as it makes it possible to determine the direction of vibration at a given frequency and the form of deformation of the robot arm. In addition, the advantage of this technique is the ability to select any number of points for analysis after image acquisition, even without prior use of markers. Disadvantages include the sensitivity of the method to lighting, as is the case with most vision techniques.

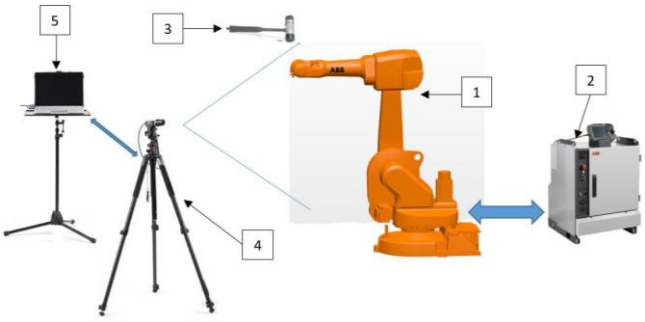

Fig. 6. Schematic diagram of the test stand: 1 – IRB 1600 robot, 2 – IRC5 controller, 3 – Impact hammer, 4 – camera, 5 – computer with RDI Motion Amplification software

The duration of a single image acquisition was 5 s at 140 frames per second and 1920 x 1200 resolution. Accordingly, the spectral analysis of vibrations was conducted in the frequency range of 0–70 Hz, and the frequency resolution of the spectral analysis was 0.2 Hz.

Fig. 7 shows selected configurations of the robot. The tests were carried out in configurations falling within the range of angle $\beta_2 \in -2{,}269 \div 2{,}619$ rad for $\beta_1 = 2\pi/3$.

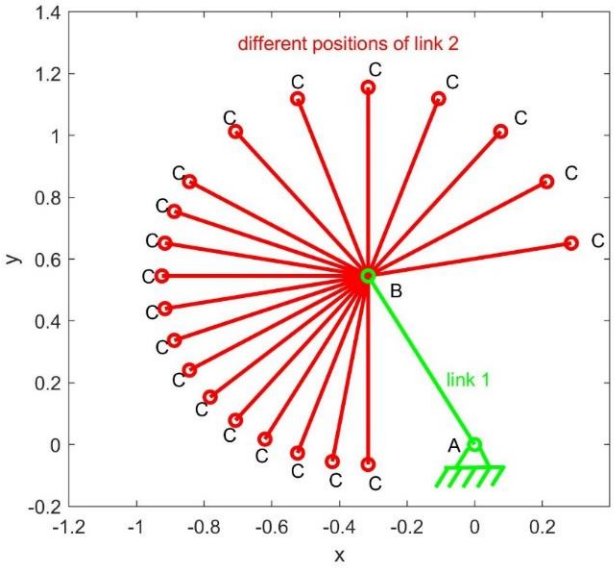

Fig. 7. Tested robot configurations

Based on the conducted tests, the characteristics of the excited vibration frequencies on the real object were obtained. The results of simulation and experimental studies are presented in Tab. 2. Fig. 8 presents a comparison of the results obtained from simulation studies (Fig. 5) and experimental studies. Since the vibration amplitudes of the links during the experiments and simulations have different values, and they are not significant in the presented studies, the results are presented in a two-dimensional graph. The values of the resonant frequencies obtained from the simulation (corresponding to the graphs in Fig. 5) are marked with the symbols "•" and "*", while the data from experimental studies are marked with the symbols "○" and "□".

The graphs shown in Fig. 8 confirm that the obtained results of simulation studies were confirmed by experimental studies. The obtained characteristics of the resonant frequencies in the studied range differ slightly from each other.

Tab. 2. Values of resonance frequencies obtained in simulation and experimental studies

	Simulation		Experiment	
β_2 [rad]	Frequency f_1 [Hz]	Frequency f_2 [Hz]	Frequency f_1 [Hz]	Frequency f_2 [Hz]
2.618	26.58	41.14	25.31	39.30
2.443	26.39	40.84	24.99	39.11
2.269	26.39	40.21	24.51	37.78
2.094	25.63	40.00	24.22	39.25
1.920	25.07	40.12	23.53	38.94
1.745	24.16	40.27	23.58	39.97
1.571	23.33	41.60	23.195	39.40
1.396	23.05	42.89	22.67	41.51
1.222	22.73	43.45	22.40	45.46
1.047	21.62	45.93	22.12	48.41
0.873	20.72	47.66	21.47	48.90
0.698	20.54	50.28	20.20	49.72
0.523	20.36	52.36	20.97	49.74
0.174	19.84	58.77	20.79	58.81
–0.174	20.23	60.67	19.26	60.02
–0.524	19.87	58.84	21.83	58.22
–0.873	20.40	52.44	20.11	52.15
–1.222	20.83	47.90	20.51	47.78
–1.571	22.10	44.22	22.14	44.06
–1.920	23.33	41.60	21.79	41.20
–2.269	25.07	40.12	-	-

An additional advantage of using a vision system with image filtering software is that it can generate movies containing extracted modes of resonance vibrations. There are two modes of resonance vibrations in the tested system. Fig. 9 presents one video frame, which shows the robot arm in a selected position defined by the angles $\beta_1 = 2\pi/3$ i $\beta_2 = -5\pi/9$. In addition, displacements of selected points are marked, which are proportional to the length of the arrows. Fig. 9a shows the total vibrations of the arm in a selected position, Fig. 9b shows the first mode of vibrations and Fig. 9c shows the second mode of vibrations. For better visibility, for the purposes of motion analysis, the displacements in Figs. 9b and 9c are shown on a larger scale than shown in Fig. 9a.

For the first and second modes of vibration, a plan of displacements was made. The displacement vector of point A for the i-th mode of vibration is $\bar{r}_{Ai} = 0$. The displacement $\bar{r}_{Bi}$ of point B is determined based on image analysis and is different from zero for each mode of vibration. From the displacement distribution of link 1, the angle α_{1i} was determined, describing the angular vibrations of link 1 relative to point A. The displacement of point C in the i-th mode of vibration is equal to $\bar{r}_{Ci} = \bar{r}_{Bi} + \bar{r}_{CBi}$, where $\bar{r}_{CBi}$ is the relative displacement of point C relative to point B. The introduction of the relative displacement made it possible to determine the angle of rotation α_{2i}, describing the angular vibrations of link 2 relative to point B. The performed analysis of the displacement distribution shows that the first mode of vibration consists in the rotation of the links in the same directions, while the second mode of vibration consists in the rotation of the links in opposite directions.

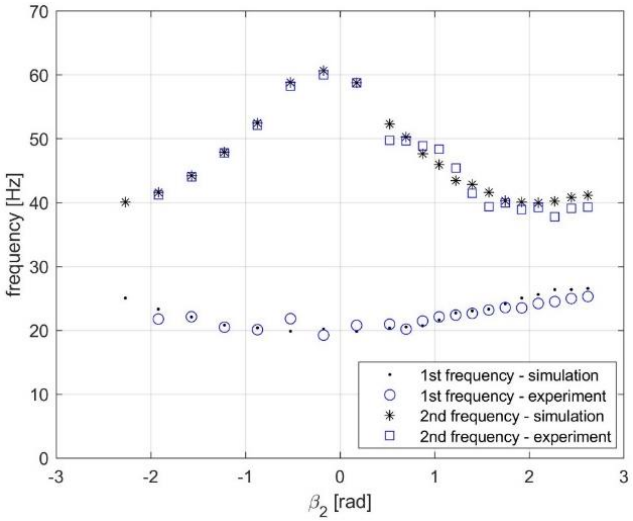

Fig. 8. Frequencies of resonant vibration in simulation and experimental studies

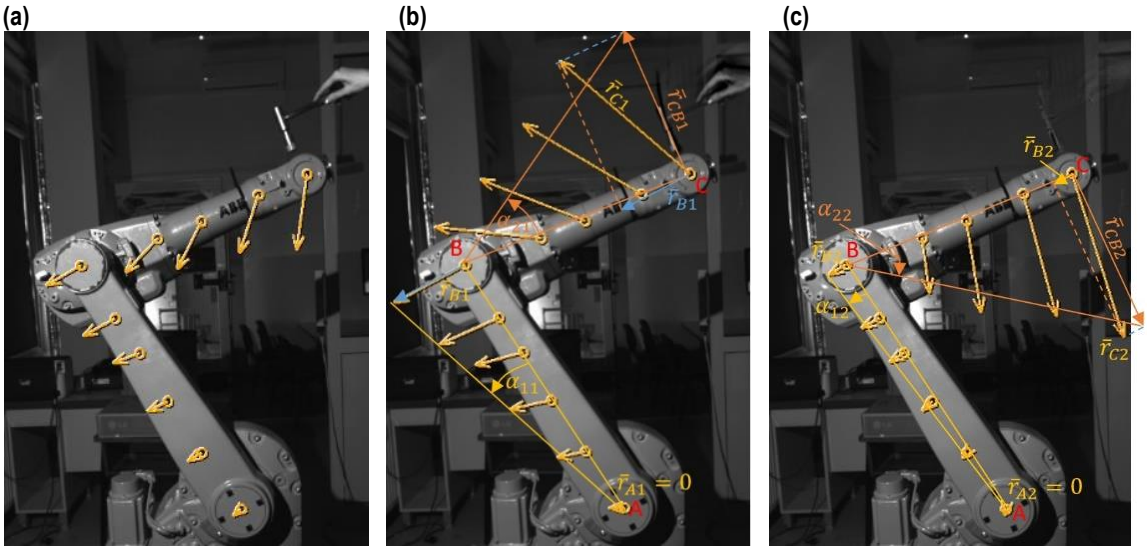

Fig. 9. Robot arm vibrations: (a) total vibrations, (b) first vibration mode, (c) second vibration mode

DOI 10.2478/ama-2023-0060

5. CONCLUSIONS

The article presents the results of a study of the dependence of the resonant frequencies of a manipulator on its configuration, understood as the angular position of the links. The dynamic equations of motion were formulated, in which only the motion of the arms related to the flexibility in the joints, that is, the motion of a vibrational nature, was taken into account, and the other effects related to the slow-moving motion of the links were omitted. From the obtained results of simulation studies, it is clear that the mutual positioning of the manipulator's links significantly affects vibration effects, including the values of resonant vibration frequencies. The results of simulation studies based on the mathematical model were confirmed by experimental studies. In addition, it should be noted that the values of resonant frequencies determined in simulation and experimental studies differ by only a few percent, with a maximum of 6.43% for the first frequency of 7.66% for the second frequency and in the configuration $\beta_2 = 2.269$ [rad].

The next stages of the research will be related to the inclusion of the arm's interaction with the environment in the mathematical model, taking into account damping and increasing the number of degrees of freedom of the manipulator model.

The equations obtained in the proposed approach, although simpler than those found in the literature, are characterised by high complexity. Their analytical solution requires the use of simplifications leading to linearisation or the use of an approximation by expanding the non-linearity into series, which will be one of the next stages of the work.

REFERENCES

1. Bauer J, Friedmann M, Hemker T, Pischan M, Reinl C, Abele E, Stryk OV. Analysis of Industrial Robot Structure and Milling Process Interaction for Path Manipulation, in: Denkena, B., Hollmann, F. (Eds.), Process Machine Interactions, Lecture Notes in Production Engineering. Springer Berlin Heidelberg, Berlin, Heidelberg, 2013; 245–263. https://doi.org/10.1007/978-3-642-32448-2_11
2. Ji W, Wang L. Industrial robotic machining: a review. Int. J. Adv. Manuf. Technol. 2019; 103, 1239–1255. https://doi.org/10.1007/s00170-019-03403-z
3. Iglesias I, Sebastián MA, Ares JE. Overview of the State of Robotic Machining: Current Situation and Future Potential. Procedia Engineering. 2015;132, 911–917. https://doi.org/10.1016/j.proeng.2015.12.577
4. Burghardt A, Szybicki D, Kurc K, Muszyńska M. Robotic Grinding Process of Turboprop Engine Compressor Blades with Active Selection of Contact Force. Teh. Vjesn. 2022; 29(1), 15-22. https://doi.org/10.17559/TV-20190710141137
5. Gierlak P. Adaptive Position/Force Control of a Robotic Manipulator in Contact with a Flexible and Uncertain Environment. Robotics. 2021; 10, 32. https://doi.org/10.3390/robotics10010032
6. Bisu C, Cherif M, Gerard A. K'nevez JY. Dynamic Behavior Analysis for a Six Axis Industrial Machining Robot. 2011; AMR 423, 65–76. https://doi.org/10.4028/www.scientific.net/AMR.423.65
7. Huynh HN, Assadi H, Rivière-Lorphèvre E, Verlinden O, Ahmadi K. Modelling the dynamics of industrial robots for milling operations. Robot. Comput-Integr. Manuf. 2020; 61, 101852. https://doi.org/10.1016/j.rcim.2019.101852
8. Nguyen V, Johnson J, Melkote S. Active vibration suppression in robotic milling using optimal control. Int. J. Mach. Tools Manuf. 2020; 152, 103541. https://doi.org/10.1016/j.ijmachtools.2020.103541
9. Busch M, Schnoes F, Elsharkawy A, Zaeh MF. Methodology for model-based uncertainty quantification of the vibrational properties of machining robots. Robot. Comput-Integr. Manuf. 2022; 73, 102243. https://doi.org/10.1016/j.rcim.2021.102243
10. Tunc LT, Gonul B. Effect of quasi-static motion on the dynamics and stability of robotic milling. 2021; CIRP Annals 70, 305–308. https://doi.org/10.1016/j.cirp.2021.04.077
11. İlman MM, Yavuz Ş, Karagülle H, Uysal A. Hybrid vibration control of an industrial CFRP composite robot-manipulator system based on reduced order model. Simulation Modelling Practice and Theory, 2022; 115: 102456. https://doi.org/10.1016/j.simpat.2021.102456
12. İlman MM, Yavuz Ş, Yildirim TP. Generalized input preshaping vibration control approach for multi-link flexible manipulators using-machine intelligence. Mechatronics, 2022; 82: 102735. doi.org/10.1016/j.mechatronics.2021.102735
13. Dwivedy SK, Eberhard P. Dynamic analysis of flexible manipulators, a literature review. Mech. Mach. 2006; Theory 41, 749–777. https://doi.org/10.1016/j.mechmachtheory.2006.01.014
14. Siciliano B, Wit CC, Bastin G. Theory of Robot Control. Springer Science & Business Media. 2012.
15. Goldsmith PB, Francis BA, Goldenberg AA. Stability of hybrid position/force control applied to manipulators with flexible joints. Int. J. Robot. Autom. 1999; 14(4), 146-160.
16. Vukobratovic M, Potkonjak V, Matijevic V. Dynamics of Robots with Contact Tasks. Springer Netherlands, Dordrecht. 2003. https://doi.org/10.1007/978-94-017-0397-0
17. Zhu Q, Mao Y, Xiong R, Wu J. Adaptive Torque and Position Control for a Legged Robot Based on a Series Elastic Actuator. Int. J. Adv. Robot. Syst. 2016; 13, 26. https://doi.org/10.5772/62204
18. Do T.-T, Vu V.-H, Liu Z. Linearization of dynamic equations for vibration and modal analysis of flexible joint manipulators. Mech. Mach. 2022; Theory 167, 104516. https://doi.org/10.1016/j.mechmachtheory.2021.104516
19. Endo T, Kawasaki H. Bending moment-based force control of flexible arm under gravity. Mech. Mach. 2014; Theory 79, 217–229. https://doi.org/10.1016/j.mechmachthory.2014.04.013
20. Cheong J, Youm Y. System mode approach for analysis of horizontal vibration of 3-D two-link flexible manipulators. J. Sound Vib. 2003; 268, 49–70. https://doi.org/10.1016/S0022-460X(02)01474-8
21. Thomsen DK, Søe-Knudsen R, Balling O, Zhang X. Vibration control of industrial robot arms by multi-mode time-varying input shaping. Mech. Mach. 2021; Theory 155, 104072. https://doi.org/10.1016/j.mechmachtheory.2020.104072
22. Yavuz Ş, İlman M. M. Modified reduced-order modeling of a flexible robot-manipulator and model-associative vibration control implementation. Extreme Mechanics Letters. 2020; 37, 100723.
23. Khorasani K. Adaptive control of flexible joint robots. Proceedings. 1991 IEEE International Conference on Robotics and Automation, Sacramento, CA, USA, 1991; vol.3, 2127-2134. https://doi: 10.1109/ROBOT.1991.131942
24. Mejri S, Gagnol V, Le TP, Sabourin L, Ray P. Dynamic characterization of machining robot and stability analysis. Int J Adv Manuf Technol 82, 2016; 351–359. https://doi.org/10.1007/s00170-015-7336-3

Paulina Pietruś: https://orcid.org/0000-0002-6428-0959

Piotr Gierlak: https://orcid.org/0000-0003-4545-8253